ELSEVIER

Comput. Methods Appl. Mech. Engrg. 190 (2001) 4649–4662

Computer methods in applied mechanics and engineering

www.elsevier.com/locate/cma

A study on the bearing contact of roller gear cams

Jie-Shing Lo, Ching-Haun Tseng *, Chung-Biau Tsay

Department of Mechanical Engineering, National Chiao Tung University, 1001 Ta Hsueh Rd, Hsinchu 30050, Taiwan, ROC

Received 22 February 2000

Abstract

This study presents contact ellipse characteristics of the roller gear cams consisting of cambered rollers and screw cam surfaces. Principal curvatures and directions of generated cam surfaces are studied. The dimensions and the directions of contact ellipses are also evaluated. The investigation results are most helpful to understand contact nature, and contact stresses of the roller gear cam, which may be considered as design indices for performance consideration.

1. Introduction

Roller gear cams are widely used in the industry for indexing. Compared with conventional indexing cams, roller gear cams require less space and provide accurate, high-speed motions. To date, most studies have been devoted to developing generation models based on the ideal condition of line contact between the cylindrical-type of cutters and cam surfaces. However, due to manufacturing and assembly errors, contacts of a roller gear cam become point contacts rather than line contacts.

Some researchers have put their efforts into setting up generation models for line-contact cases [1–6]. The cylindrical-type of cutter is most frequently used for generation of cam surfaces [1]. However, several types of cutters can be selected for the cam surface generation. Chakraborty and Dhande [2] introduced several types of followers for generating the three-dimensional cam surfaces by applying the screw theory. Yan and Chen [3–5] proposed conical and hyperboloidal types of roller followers to reduce the contact surface sliding phenomena in the generation of the roller gear cam, however, they did not study their contact characteristics and pre-load advantages.

The operating performance of a roller gear cam depends on its geometry and kinematic characteristics. Yan and Chen [3–5], and Tsay and Lin [6] presented geometric models of the roller gear cam with line contact. Tsay and Lin [6] evaluated the normal curvatures of cam surfaces. Yan and Chen [3,4] presented a formula for calculating the undercut conditions of generated cam surfaces. Oizumi and Emura [7] proposed a globoidal-cam worm gear transmission assemblage using two roller-wheels to adjust pre-loading. However, all of these studies were based on the line-contact model of the roller gear cam. Since kinematic and dynamic effects are ineluctable due to manufacturing and assembly errors, contacts of a roller gear cam may become point contacts at the edges of the cam surfaces. When the contact point moves to the edge of a cam or follower, a high contact stress is induced which may result in wearing or failure of the cam surfaces. Therefore, the roller profile should be modified to ensure that the contact point is located within the widths of cam tracks, and contact ellipses are not truncated at the edge of cam surfaces.

* Corresponding author. Tel.: +886-35-5726111 ext. 55129; fax: +886-35-717243.
E-mail address: chtseng@cc.nctu.edu.tw (C.-H. Tseng).

0045-7825/01/$ - see front matter
PII: S0045-7825(00)00337-6

Litvin [8] proposed the generation of conjugate surfaces and investigated the meshing properties of spatial gearing with point contact. According to the concept of point contact, Litvin and Tsay [9] established a numerical method for simulating the conditions of meshing and bearing contact. Litvin et al. [10] also studied the relationship between curvatures and contact ellipses for conjugate gear-tooth surfaces. Wang et al. [11] studied a roller with a modified constant-radius crowned profile to simulate the contact between roller and cam surfaces. However, the characteristics of the contact ellipse between cambered rollers and cam surfaces have not been studied. Since the angular displacements of output turrets are not constant functions of input angular displacements of cam axes, the principal curvatures and directions of cam profiles have to be modified as proposed by Litvin for gearing design. In this study, a roller gear cam mechanism with point contact is investigated. Principle curvatures and directions of the roller follower and cam surfaces are studied. The dimensions and orientation of the contact ellipse are also investigated. The results are most helpful for designing the roller gear cam mechanisms.

2. Mathematical model of the roller

A cylindrical roller-type cutter is usually used for cam surface generation. The coordinate systems selected for the cam surface generation are shown in Fig. 1, where coordinate systems $S_1(X_1, Y_1, Z_1)$, $S_2(X_2, Y_2, Z_2)$ and $S_f(X_f, Y_f, Z_f)$ are attached to the follower, cam, and frame of the roller gear cam mechanism, respectively. In Fig. 1, X_c is the shortest distance of the turret and the cam axes, $l_{\min}$ and $l_{\max}$ the top and bottom bounds of the roller-type cutter, r the radius of the cutter, and $S(\phi)$ is the angular displacement function of the turret with respect to the rotation angle of the cam axis ϕ. Fig. 2 shows the coordinate system and design parameters of the roller-type cutter. The position vector of the roller-type cutter can be represented in coordinate system S_1 as follows:

$$\mathbf{\Sigma}_1^{(1)} = \begin{bmatrix} l \\ r\cos\theta \\ r\sin\theta \end{bmatrix}. \tag{1}$$

The locus of the cylindrical-type cutter can be transformed into the fixed frame coordinate system S_f as follows:

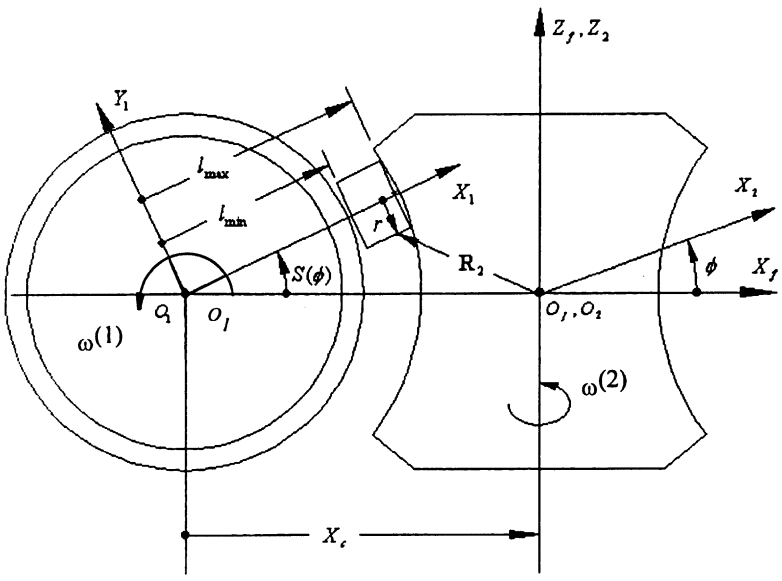

Fig. 1. The coordinate system of the roller gear cam mechanism.

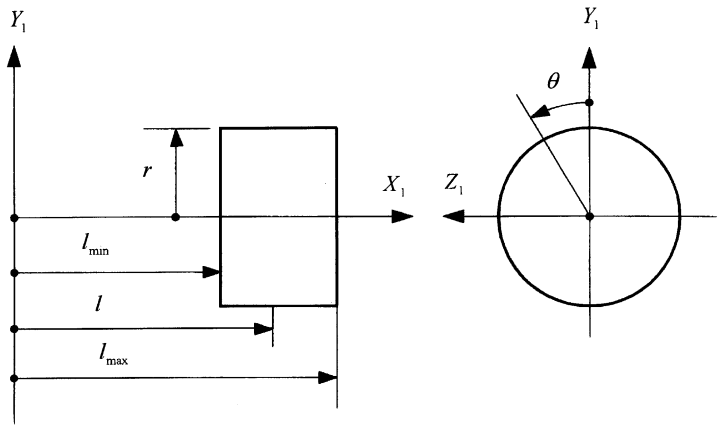

Fig. 2. Coordinate system and design parameters of the roller-type cutter.

$$\mathbf{\Sigma}_1^{(1)} = \begin{bmatrix} l\cos S - r\sin S\cos\theta - X_c \\ -r\sin\theta \\ l\sin S + r\cos S\cos\theta \end{bmatrix}, \tag{2}$$

where parameters l and θ are the surface coordinates of the roller-type cutter. The unit normal vector $\mathbf{n}_f^{(1)}$ of the roller-type cutter $\mathbf{\Sigma}_f^{(1)}$ can be obtained from

$$\mathbf{n}_f^{(1)} = \frac{\partial\mathbf{\Sigma}_f^{(1)}/\partial l \times \partial\mathbf{\Sigma}_f^{(1)}/\partial\theta}{\left|\partial\mathbf{\Sigma}_f^{(1)}/\partial l \times \partial\mathbf{\Sigma}_f^{(1)}/\partial\theta\right|} = \begin{bmatrix} -\sin S\cos\theta \\ -\sin\theta \\ \cos S\sin\theta \end{bmatrix}. \tag{3}$$

3. Equation of meshing for the roller and cam

If $\mathbf{V}_f^{(1)}$ and $\mathbf{V}_f^{(2)}$, respectively, represent the velocity vectors of the instantaneous contact point (or contact line) on the cutter and cam surfaces, expressed in the fixed coordinate system S_f, then the relative sliding velocity $\mathbf{V}_f^{(12)}$ between the cutter and cam surfaces at the contact point can be derived as follows:

$$\mathbf{V}_f^{(12)} = \mathbf{V}_f^{(1)} - \mathbf{V}_f^{(2)} = \boldsymbol{\omega}^{(12)} \times \mathbf{\Sigma}_f^{(1)} - X_c\mathbf{i}_f \times \boldsymbol{\omega}^{(2)} = \omega^2 \begin{bmatrix} rS'\cos S\cos\theta + lS'\sin S - r\sin\theta \\ r\sin S\cos\theta - l\cos S + X_c \\ rS'\sin S\cos\theta - lS'\cos S \end{bmatrix} \tag{4}$$

where

$$\boldsymbol{\omega}^{(1)} = \frac{\mathrm{d}\mathbf{S}}{\mathrm{d}t} = \frac{\mathrm{d}\mathbf{S}}{\mathrm{d}\phi}\frac{\mathrm{d}\phi}{\mathrm{d}t} = S'\omega^{(2)}\mathbf{j}, \quad \boldsymbol{\omega}^{(2)} = \omega^{(2)}\mathbf{k}, \quad \text{and } \boldsymbol{\omega}^{(12)} = \boldsymbol{\omega}^{(1)} - \boldsymbol{\omega}^{(2)}, \tag{5}$$

where $\boldsymbol{\omega}^{(1)}$ and $\boldsymbol{\omega}^{(2)}$ are the angular velocities of the turret and the cam, respectively, S' the partial derivative of the angular displacement function S with respect to cam rotation ϕ and $\mathbf{k}$ is the unit direction of the turret rotation axis. The equation of meshing [9] ensures continuous tangency of the two contact mating surfaces and can be represented by

$$f(l,\theta) = \mathbf{n}_f^{(1)} \cdot \mathbf{V}_f^{(12)} = 0. \tag{6}$$

Eq. (6) indicates that the unit normal $\mathbf{n}_f^{(1)}$ of the cutter surface and the relative velocity $\mathbf{V}_f^{(12)}$ of the cutter and cam surfaces are mutually perpendicular. Eq. (6) is the so-called equation of meshing for cylindrical-type of cutter and generated cam surfaces.

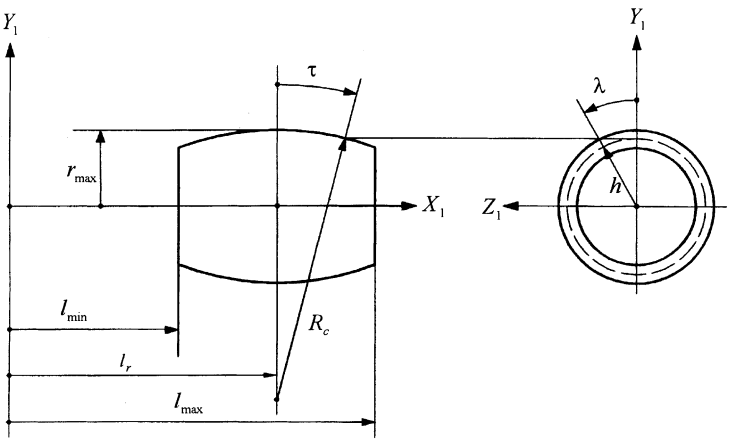

Fig. 3. Coordinate system and design parameters of the camber roller.

4. Profile of the cambered roller

In order to design a roller-cam mechanism with point contact, a cambered roller, as shown in Fig. 3, was adopted. Parameter h represents the radius of the cambered roller follower as measured from the center of the roller to the contact point on the surface $\mathbf{\Sigma}_1^{(h)}$ represented in the S_1 coordinate system. The angle λ is the contact angle measured from the Y_1-axis to the contact point, the symbol R_c the radius of the crowned roller surface, r_{max} the maximum roller radius of h, and l_r is the surface coordinates of the cambered roller measured along the turret rotation axis. According to the geometric relationship shown in Fig. 3, the profile of the cambered roller can be expressed in the coordinate system S_1 as follows:

$$\mathbf{\Sigma}_1^{(h)} = \begin{bmatrix} l_r + R_c \sin\tau \\ h\cos\lambda \\ h\sin\lambda \end{bmatrix}, \tag{7}$$

where $h = R_c(\cos\tau - 1) + r_{max}$, and parameters τ and λ are the surface coordinates of the cambered roller surface. The left and right bounds of τ are defined as

$$\sin^{-1}\left(\frac{l_{min} - l_r}{R_c}\right) \leqslant \tau \leqslant \sin^{-1}\left(\frac{l_{max} - l_r}{R_c}\right). \tag{8}$$

The unit normal $\mathbf{n}_1^{(h)}$ of the cambered roller surface can be obtained from

$$\mathbf{n}_1^{(h)} = \frac{\partial\mathbf{\Sigma}_1^{(h)}/\partial\tau \times \partial\mathbf{\Sigma}_1^{(h)}/\partial\lambda}{\left|\partial\mathbf{\Sigma}_1^{(h)}/\partial\tau \times \partial\mathbf{\Sigma}_1^{(h)}/\partial\lambda\right|} = \begin{bmatrix} \sin\tau \\ \cos\tau\cos\lambda \\ \cos\tau\sin\lambda \end{bmatrix}. \tag{9}$$

The surface unit normal $\mathbf{n}_1^{(h)}$ can also be translated into coordinate system S_f by applying the following matrix transformation equation:

$$\mathbf{n}_f^{(h)} = \begin{bmatrix} \cos S & -\sin S & 0 \\ 0 & 0 & -1 \\ \sin S & \cos S & 0 \end{bmatrix} \mathbf{n}_1^{(h)} = \begin{bmatrix} \cos S\sin\tau - \sin S\cos\tau\cos\lambda \\ -\cos\tau\sin\lambda \\ \sin S\sin\tau + \cos S\cos\tau\cos\lambda \end{bmatrix}. \tag{10}$$

5. Principal curvatures and directions of cylindrical roller-type cutters

Since the profile of the proposed roller has a crowned surface, the bearing contact of the roller gear cam becomes point contact instead of line contact. Due to the elasticity of the cam and roller surfaces, under

loading, the contact between these two mating surfaces is spread over an elliptical area. The principal curvatures and directions of the roller and cam surfaces, which are necessary for evaluating lubrication conditions, contact stresses, and deformations, are investigated to define the size and the orientation of the contact ellipse on the contact surface.

For convenience of expression, the symbol $\mathbf{r}^{(1)}$ represents the position vector of the cylindrical roller-type cutter $\mathbf{\Sigma}_f^{(1)}$ expressed in Eq. (1). The principal curvatures $\kappa_f^{(1)}$ and $\kappa_h^{(1)}$ of the cutter surface satisfy the Rodrigues' equation [9]:

$$\kappa_{f,h}^{(1)}\mathbf{V}_{\mathrm{r}} = -\dot{\mathbf{n}}_{\mathrm{r}}, \tag{11}$$

where $\mathbf{V}_{\mathrm{r}}$ is the relative velocity at the contact point, $\dot{\mathbf{n}}_{\mathrm{r}}$ the velocity of the tip of the cam surface unit normal, and superscript "1" represents the surface of the roller cutter. The principle directions at roller-type cutter point P coincide with the tangent lines $\mathbf{r}_l^{(1)}$ and $\mathbf{r}_\theta^{(1)}$ on the roller surface. Eqs. (2), (3) and (11) yield that:

1. For the case of $\mathrm{d}\theta = 0$, the first principal direction $\mathbf{e}_f^{(1)}$ and curvature $\kappa_f^{(1)}$ are given as follows:

$$\mathbf{e}_f^{(1)} = \frac{\mathbf{r}_l^{(1)}}{\left|\mathbf{r}_l^{(1)}\right|} = \begin{bmatrix} 1 \\ 0 \\ 0 \end{bmatrix} \quad \text{and} \quad \kappa_f^{(1)} = 0. \tag{12}$$

2. For the case $\mathrm{d}l = 0$, the second principal direction $\mathbf{e}_h^{(1)}$ and curvature $\kappa_h^{(l)}$ are obtained as follows:

$$\mathbf{e}_h^{(1)} = \frac{\mathbf{r}_\theta^{(1)}}{\left|\mathbf{r}_\theta^{(1)}\right|} = \begin{bmatrix} 0 \\ -\sin\theta \\ \cos\theta \end{bmatrix} \quad \text{and} \quad \kappa_h^{(1)} = \frac{1}{r}. \tag{13}$$

The principal directions $\mathbf{e}_f^{(1)}$ and $\mathbf{e}_h^{(1)}$, as well as the corresponding principle curvatures $\kappa_h^{(1)}$ and $\kappa_h^{(1)}$ of the cylindrical roller-type cutter, represented in Eqs. (12) and (13) are expressed in the coordinate system $S_1(X_1, Y_1, Z_1)$. The principal directions can also be represented in the coordinate system $S_f(X_f, Y_f, Z_f)$ by pre-multiplying the transformation matrix as follows:

$$L_{f1} = \begin{bmatrix} \cos S & -\sin S & 0 \\ 0 & 0 & -1 \\ \sin S & \cos S & 0 \end{bmatrix}. \tag{14}$$

6. Principal curvatures and directions of the generated cam surface

The cylindrical roller-type cutter generates the cam surface, which means that the roller-type cutter $\mathbf{\Sigma}_f^{(1)}$ and the cam surface $\mathbf{\Sigma}_f^{(2)}$ are in line contact during the process of generation. It is assumed that the principal curvatures $\kappa_f^{(1)}$ and $\kappa_f^{(1)}$, as well as the corresponding principal directions $\mathbf{e}_f^{(1)}$ and $\mathbf{e}_h^{(1)}$ of the roller-type cutter $\mathbf{\Sigma}_f^{(1)}$ at the contact position P are given, and the motion parameters at all instantaneous points are also known. Our goal is to determine the principal curvatures $\kappa_s^{(2)}$ and $\kappa_q^{(2)}$, and the corresponding principal directions, $\mathbf{e}_s^{(2)}$, $\mathbf{e}_q^{(2)}$, of the generated cam surface $\mathbf{\Sigma}_f^{(2)}$. Fig. 4 shows the relationship between the principal directions of $\mathbf{\Sigma}_f^{(1)}$ and $\mathbf{\Sigma}_f^{(2)}$. Angle σ is formed by the unit vectors $\mathbf{e}_f^{(1)}$ and $\mathbf{e}_s^{(2)}$ of the first principal directions of the roller-type cutter surface and the generated cam surface, and is measured counterclockwise from $\mathbf{e}_f^{(1)}$ to $\mathbf{e}_s^{(2)}$. The coordinate transformation between coordinate systems $S_a(\mathbf{e}_f^{(1)}, \mathbf{e}_h^{(1)})$ and $S_b(\mathbf{e}_s^{(2)}, \mathbf{e}_q^{(2)})$ is expressed as follows:

$$\mathbf{L}_{ab} = \begin{bmatrix} \cos\sigma & -\sin\sigma & 0 \\ \sin\sigma & \cos\sigma & 0 \\ 0 & 0 & 1 \end{bmatrix},$$

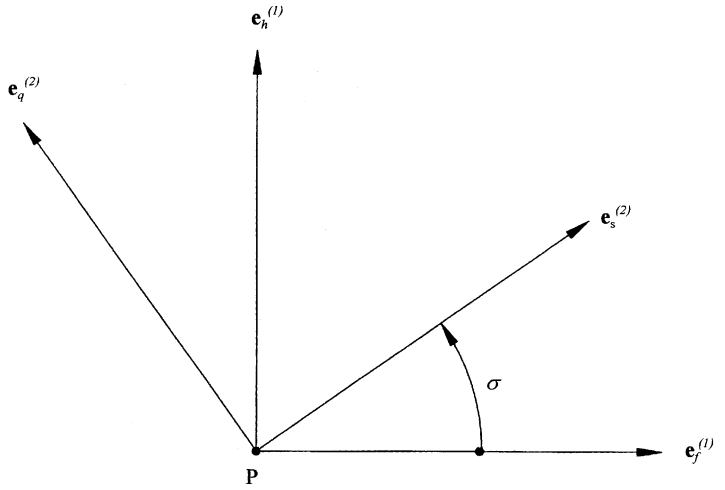

Fig. 4. Principal directions of roller and cam surfaces.

and

$$\mathbf{L}_{ba} = \begin{bmatrix} \cos\sigma & \sin\sigma & 0 \\ -\sin\sigma & \cos\sigma & 0 \\ 0 & 0 & 1 \end{bmatrix}. \tag{15}$$

Two mating conjugate surfaces must satisfy the condition of continuous tangency, therefore, the following relationships must be maintained [10]:

$$\mathbf{r}^{(1)}(l_1, \theta_1, S) = \mathbf{r}^{(2)}(l_2, \theta_2, \phi), \tag{16}$$

and

$$\mathbf{n}^{(1)}(l_1, \theta_1, S) = \mathbf{n}^{(2)}(l_2, \theta_2, \phi), \tag{17}$$

where $\mathbf{r}^{(1)}$ is the position vector of the cylindrical roller-type cutter measured from the origin of the coordinate system S_f to the contact point, $\mathbf{r}^{(2)}$ the position vector of the generated cam surface, correspondingly, $\mathbf{n}^{(1)}$ and $\mathbf{n}^{(2)}$ the surface unit normal parameters, l and θ the surface coordinates, S the angular displacement of the turret and ϕ is the angular displacement of the camshaft. In the designing of roller gear cam, $S(\phi) \in C^2$ is given. Due to the requirement for continuous tangency between the roller and cam surfaces [10], the following conditions are also maintained in the neighborhood of contact point P:

$$\dot{\mathbf{r}}^{(1)}(l_1, \theta_1, S) = \dot{\mathbf{r}}^{(2)}(l_2, \theta_2, \phi), \tag{18}$$

$$\dot{\mathbf{n}}^{(1)}(l_1, \theta_1, S) = \dot{\mathbf{n}}^{(2)}(l_2, \theta_2, \phi), \tag{19}$$

and

$$\frac{\mathrm{d}}{\mathrm{d}t}\left(\mathbf{n}^{(1)} \cdot \mathbf{V}^{(12)}\right) = 0. \tag{20}$$

Eqs. (18) and (19) yield the following relationships [9]:

$$\mathbf{V}_{\mathrm{r}}^{(2)} = \mathbf{V}_{\mathrm{r}}^{(1)} + \mathbf{V}^{(12)}, \tag{21}$$

and

$$\dot{\mathbf{n}}_{\mathrm{r}}^{(2)} = \dot{\mathbf{n}}_{\mathrm{r}}^{(1)} + \left(\boldsymbol{\omega}^{(12)} \times \mathbf{n}\right), \tag{22}$$

where the subscript r indicates the velocity at the contact point in relative motion over the surface, $\mathbf{V}^{(12)}$ the sliding velocity at the point of surface tangency and $\mathbf{n}$ is the surface unit normal at the corresponding contact point. Eqs. (21) and (22), expressed in the coordinate systems $\mathbf{S}_a(e_f^{(1)}, e_h^{(1)})$ and $\mathbf{S}_b(e_s^{(2)}, e_q^{(2)})$, yield [10]

$$\begin{bmatrix} v_f^{(2)} \\ v_h^{(2)} \end{bmatrix} = \begin{bmatrix} v_f^{(1)} \\ v_h^{(1)} \end{bmatrix} + \begin{bmatrix} v_f^{(12)} \\ v_h^{(12)} \end{bmatrix}, \tag{23}$$

$$\begin{bmatrix} \dot{\mathbf{n}}_f^{(2)} \\ \dot{\mathbf{n}}_h^{(2)} \end{bmatrix} = \begin{bmatrix} \dot{\mathbf{n}}_f^{(1)} \\ \dot{\mathbf{n}}_h^{(1)} \end{bmatrix} + \begin{bmatrix} (\boldsymbol{\omega}^{(12)} \times \mathbf{n}) \cdot \mathbf{e}_f \\ (\boldsymbol{\omega}^{(12)} \times \mathbf{n}) \cdot \mathbf{e}_h \end{bmatrix}, \tag{24}$$

$$\begin{bmatrix} v_s^{(2)} \\ v_q^{(2)} \end{bmatrix} = \begin{bmatrix} v_s^{(1)} \\ v_q^{(1)} \end{bmatrix} + \begin{bmatrix} v_s^{(12)} \\ v_q^{(12)} \end{bmatrix}, \tag{25}$$

and

$$\begin{bmatrix} \dot{\mathbf{n}}_s^{(2)} \\ \dot{\mathbf{n}}_q^{(2)} \end{bmatrix} = \begin{bmatrix} \dot{\mathbf{n}}_s^{(1)} \\ \dot{\mathbf{n}}_q^{(1)} \end{bmatrix} + \begin{bmatrix} (\boldsymbol{\omega}^{(12)} \times \mathbf{n}) \cdot \mathbf{e}_s \\ (\boldsymbol{\omega}^{(12)} \times \mathbf{n}) \cdot \mathbf{e}_q \end{bmatrix}. \tag{26}$$

Vectors $\mathbf{V}_{\mathrm{r}}^{(i)}$ and $\dot{\mathbf{n}}_{\mathrm{r}}^{(i)}$, $(i = 1, 2)$, and Eq. (11) yield that

$$\begin{bmatrix} \dot{\mathbf{n}}_f^{(1)} \\ \dot{\mathbf{n}}_h^{(1)} \end{bmatrix} = \begin{bmatrix} -\kappa_f & 0 \\ 0 & -\kappa_h \end{bmatrix} \begin{bmatrix} v_f^{(1)} \\ v_h^{(1)} \end{bmatrix} = \mathbf{K}_1 \begin{bmatrix} v_f^{(1)} \\ v_h^{(1)} \end{bmatrix}, \tag{27}$$

and

$$\begin{bmatrix} \dot{\mathbf{n}}_s^{(2)} \\ \dot{\mathbf{n}}_q^{(2)} \end{bmatrix} = \begin{bmatrix} -\kappa_s & 0 \\ 0 & -\kappa_q \end{bmatrix} \begin{bmatrix} v_s^{(2)} \\ v_q^{(2)} \end{bmatrix} = \mathbf{K}_2 \begin{bmatrix} v_s^{(2)} \\ v_q^{(2)} \end{bmatrix}. \tag{28}$$

The Rodrigue's formula and coordinate transformation matrix equations (27) and (28) result in:

$$\begin{bmatrix} \dot{\mathbf{n}}_f^{(2)} \\ \dot{\mathbf{n}}_h^{(2)} \end{bmatrix} = \mathbf{L}_{ab}\mathbf{K}_2\mathbf{L}_{ba} \begin{bmatrix} v_f^{(2)} \\ v_h^{(2)} \end{bmatrix}. \tag{29}$$

Substituting Eqs. (21), (27) and (29) into Eq. (24) yield that

$$(\mathbf{K}_1 - \mathbf{L}_{ab}\mathbf{K}_2\mathbf{L}_{ba}) \begin{bmatrix} v_f^{(2)} \\ v_h^{(2)} \end{bmatrix} = \mathbf{K}_1 \begin{bmatrix} v_f^{(12)} \\ v_h^{(12)} \end{bmatrix} + \begin{bmatrix} (\mathbf{n}^{(1)} \times \boldsymbol{\omega}^{(12)}) \cdot \mathbf{e}_f^{(1)} \\ (\mathbf{n}^{(1)} \times \boldsymbol{\omega}^{(12)}) \cdot \mathbf{e}_h^{(1)} \end{bmatrix}. \tag{30}$$

Eq. (30) contains two linear equations with two unknowns $\mathbf{v}_f^{(2)}$ and $\mathbf{v}_h^{(2)}$.

We now consider Eq. (20) and rewrite it as follows:

$$\dot{\mathbf{n}}^{(1)} \cdot \mathbf{V}_f^{(12)} + \mathbf{n}^{(1)} \cdot \left[\left(\boldsymbol{\omega}^{(1)} \times \mathbf{r}^{(1)} \right) + \boldsymbol{\omega}^{(12)} \times \dot{\mathbf{r}}^{(1)} \right] = 0. \tag{31}$$

According to differential geometry, it is known that [8]:

$$\dot{\mathbf{n}}^{(1)} = \mathbf{n}_{\mathrm{r}}^{(1)} + \left(\boldsymbol{\omega}^{(1)} \times \mathbf{n} \right), \tag{32}$$

and

$$\dot{\mathbf{r}}^{(1)} = \mathbf{V}_{\mathrm{r}}^{(1)} + \mathbf{V}_{\mathrm{tr}}^{(1)}, \tag{33}$$

where subscripts r and tr indicate the velocity of the contact point in relative motion (over the surface) and in transfer motion (with the surface), respectively. Substituting Eqs. (32) and (33) into Eq. (31) and using certain mathematical operations yield that

$$\dot{\mathbf{n}}_{\mathrm{r}}^{(1)} \cdot \mathbf{V}^{(12)} + \mathbf{V}_{\mathrm{r}}^{(1)} \cdot \left(\mathbf{n}^{(1)} \times \boldsymbol{\omega}^{(12)}\right) + \mathbf{n}^{(1)} \cdot \left[\left(\boldsymbol{\omega}^{(1)} \times \mathbf{V}_{\mathrm{tr}}^{(2)}\right) - \left(\boldsymbol{\omega}^{(2)} \times \mathbf{V}_{\mathrm{tr}}^{(1)}\right) + \left(\dot{\boldsymbol{\omega}}^{(1)} \times \mathbf{r}^{(1)}\right)\right] = 0. \tag{34}$$

Substituting Eqs. (11) and (21) into Eq. (34), one obtains a system of two equations with two unknowns, $\mathbf{v}_f^{(2)}$ and $\mathbf{v}_h^{(2)}$:

$$\begin{aligned}
&\left\{ \begin{bmatrix} v_f^{(12)} \\ v_h^{(12)} \end{bmatrix}^{\mathrm{T}} \mathbf{K}_1 + \begin{bmatrix} \left(\mathbf{n}^{(1)} \times \boldsymbol{\omega}^{(12)}\right) \cdot \mathbf{e}_f \\ \left(\mathbf{n}^{(1)} \times \boldsymbol{\omega}^{(12)}\right) \cdot \mathbf{e}_h \end{bmatrix}^{\mathrm{T}} \right\} \begin{bmatrix} v_f^{(2)} \\ v_h^{(2)} \end{bmatrix} \\
&\quad = \mathbf{n}^{(1)} \cdot \left[\left(\boldsymbol{\omega}^{(2)} \times \mathbf{V}_{\mathrm{tr}}^{(1)}\right) - \left(\boldsymbol{\omega}^{(1)} \times \mathbf{V}_{\mathrm{tr}}^{(2)}\right) - \left(\dot{\boldsymbol{\omega}}^{(1)} \times \mathbf{r}^{(1)}\right)\right] \\
&\qquad + \left(\mathbf{n}^{(1)} \times \boldsymbol{\omega}^{(12)}\right) \cdot \mathbf{V}_f^{(12)} - \kappa_f^{(1)} (\mathbf{V}_f^{(12)})^2 - \kappa_h^{(1)} (\mathbf{V}_h^{(12)})^2.
\end{aligned} \tag{35}$$

Eqs. (30) and (35) comprise a system of three linear equations in two unknowns $\mathbf{V}_f^{(2)}$, and $\mathbf{V}_h^{(2)}$. The requirement for solving the system equation to derive a unique solution is that the rank of the system equations should be two. This condition enables to obtain the following equations for the principal curvatures and directions of the generated cam surface $\boldsymbol{\Sigma}_f^{(2)}$:

$$\tan 2\sigma = \frac{2 t_{13} t_{23}}{t_{23}^2 - t_{13}^2 - (\kappa_f^{(1)} - \kappa_h^{(1)}) t_{33}}, \tag{36}$$

$$\kappa_q^{(2)} - \kappa_s^{(2)} = \frac{t_{23}^2 - t_{13}^2 - (\kappa_f^{(1)} - \kappa_h^{(1)}) t_{33}}{t_{33} \cos 2\sigma}, \tag{37}$$

and

$$\kappa_s^{(2)} + \kappa_q^{(2)} = \kappa_f^{(1)} + \kappa_h^{(1)} + \frac{t_{13}^2 + t_{23}^2}{t_{33}}, \tag{38}$$

where

$$t_{13} = \left(\left(\mathbf{n}^{(1)} \times \boldsymbol{\omega}^{(12)}\right) \cdot \mathbf{e}_f^{(1)}\right) - \kappa_f \left(\mathbf{V}_f^{(12)} \cdot \mathbf{e}_f^{(1)}\right), \tag{39}$$

$$t_{23} = \left(\left(\mathbf{n}^{(1)} \times \boldsymbol{\omega}^{(12)}\right) \cdot \mathbf{e}_h^{(1)}\right) - \kappa_h \left(\mathbf{V}_f^{(12)} \cdot \mathbf{e}_h^{(1)}\right), \tag{40}$$

$$\begin{aligned}
t_{33} = {} & \mathbf{n}^{(1)} \cdot \left[\left(\boldsymbol{\omega}^{(2)} \times \mathbf{V}_{\mathrm{tr}}^{(1)}\right) - \left(\boldsymbol{\omega}^{(1)} \times \mathbf{V}_{\mathrm{tr}}^{(2)}\right) - \left(\dot{\boldsymbol{\omega}}^{(1)} \times \mathbf{r}^{(1)}\right)\right] + \left(\mathbf{n}^{(1)} \times \boldsymbol{\omega}^{(12)}\right) \cdot \mathbf{V}_f^{(12)} \\
& - \kappa_f \left(\mathbf{V}_f^{(12)}\right)^2 - \kappa_h \left(\mathbf{V}_h^{(12)}\right)^2,
\end{aligned} \tag{41}$$

and σ is the angle formed by the principal directions of the roller-type cutter and the generated cam surfaces, as shown in Fig. 4.

7. Principal curvatures and directions of the cambered roller

The Rodrigues' equation can also be used to determine the principal curvatures and directions of the cambered roller surface, $\boldsymbol{\Sigma}_1^{(h)}(\tau, \lambda)$,, where τ and λ are the surface coordinates. According to Eqs. (7), (9) and (11), the principal curvatures and directions are obtained as follows:

1. For the case of $d\lambda = 0$, the first principal direction $\mathbf{e}_f^{(h)}$ and curvature $\kappa_f^{(h)}$ are obtained from:

$$\mathbf{e}_f^{(h)} = \frac{\mathbf{r}_\tau^{(h)}}{\left|\mathbf{r}_\tau^{(h)}\right|} = \begin{bmatrix} \cos\tau \\ -\sin\tau\cos\lambda \\ -\sin\tau\sin\lambda \end{bmatrix} \quad \text{and} \quad \kappa_f^{(h)} = \frac{1}{R_c}. \tag{42}$$

2. For the case of $d\tau = 0$, the second principal direction $\mathbf{e}_h^{(h)}$ and curvature $\kappa_h^{(h)}$ are obtained from:

$$\mathbf{e}_h^{(h)} = \frac{\mathbf{r}_\lambda^{(h)}}{\left|\mathbf{r}_\lambda^{(h)}\right|} = \begin{bmatrix} 0 \\ -\sin\lambda \\ -\cos\lambda \end{bmatrix} \quad \text{and} \quad \kappa_h^{(h)} = \frac{\cos\tau}{r_{\max} + R_c(\cos\tau - 1)}. \tag{43}$$

8. Surface contact analysis

Since the roller is a crowned surface, the cambered roller and cam surfaces are in point contact. Therefore, edge contact will not occur even as a result of assembly errors and the meshing of the roller and cam surfaces will remain a point contact located near the middle region of the cam surface.

To investigate the contact of the roller gear cam, the follower surface and cam surface must be expressed in the same coordinate system, say S_f. The contact points can be found by applying the tooth contact analysis (TCA) technique [9]. At the contact point of the cambered roller and cam surfaces, the following conditions must be maintained:

$$\mathbf{r}_f^{(h)}(\tau, \lambda, \delta) = \mathbf{r}_f^{(2)}(l, \theta, S), \tag{44}$$

and

$$\mathbf{n}_f^{(h)}(\tau, \lambda, \delta) = \mathbf{n}_f^{(2)}(l, \theta, S), \tag{45}$$

where parameters τ and λ are the surface coordinates of the cambered roller surface $\mathbf{\Sigma}_f^{(h)}$, l and θ the surface coordinates of the cam surface $\mathbf{\Sigma}_f^{(2)}$, S the angular displacement of the turret during the cam surface generation process and δ is the angular displacement of the turret on the roller surface. Eq. (44) expresses that the roller surface $\mathbf{\Sigma}_f^{(h)}$ and cam surface $\mathbf{\Sigma}_f^{(2)}$ have a common contact point determined by their respective position vectors, $\mathbf{r}_f^{(h)}$ and $\mathbf{r}_f^{(2)}$. Eq. (45) indicates that the roller surface $\mathbf{\Sigma}_f^{(h)}$ and cam surface $\mathbf{\Sigma}_f^{(2)}$ have a common unit normal at their common contact points. Eqs. (44) and (45) consist of five independent equations with six unknowns, since $|\mathbf{n}_f^{(h)}| = |\mathbf{n}_f^{(2)}| = 1$. The rotation angle ϕ of the cam axis is considered as a given value, and thus $S(\phi)$ is known. The remaining five unknowns τ, λ, δ, l and θ can be determined by solving the nonlinear system equations. The contact point can be obtained by substituting the solved five unknowns into the cam surface equations. Furthermore, the displacement errors $\Delta S(\phi)$ can be obtained by:

$$\Delta S(\phi) = \delta(\phi) - S(\phi). \tag{46}$$

Consequently, the contact path and the displacement errors caused by assembly errors can be determined by applying the TCA results.

9. Contact ellipse

When the principal curvatures of the cambered roller $\kappa_f^{(h)}$ and $\kappa_h^{(h)}$ and the surface of the roller gear cam $\kappa_s^{(2)}$ and $\kappa_q^{(2)}$, and their respective principal directions $\mathbf{e}_f^{(h)}, \mathbf{e}_h^{(h)}, \mathbf{e}_s^{(2)}$ and $\mathbf{e}_q^{(2)}$, as well as the angle σ are known, then our aim is to calculate the dimension and orientation of the contact ellipse at contact point. Fig. 5 shows the dimension and orientation of the contact ellipse with respect to the principal directions of the cam and the roller. Angle α, measured counterclockwise from $\mathbf{e}_f^{(h)}$ to the minor axis η, determines the orientation of the axes η with respect to the first principal direction of the cam surface $\mathbf{e}_f^{(h)}$. The dimensions

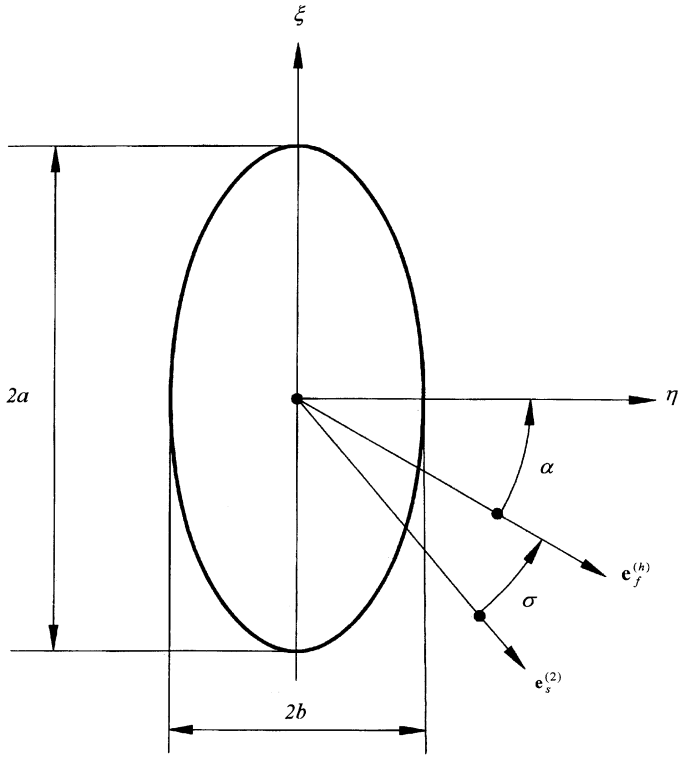

Fig. 5. Coordinate system of the contact ellipse.

and the orientation of the contact ellipse can be obtained in terms of the principal curvatures, angle α and the elastic bearing approach δ_e. The necessary calculation equations are given as below [10]

$$A = \frac{1}{4}\left[\kappa_\Sigma^{(1)} - \kappa_\Sigma^{(2)} - \left(g_1^2 - 2g_1g_2\cos 2\sigma + g_2^2\right)^{1/2}\right], \tag{47}$$

$$B = \frac{1}{4}\left[\kappa_\Sigma^{(1)} - \kappa_\Sigma^{(2)} + \left(g_1^2 - 2g_1g_2\cos 2\sigma + g_2^2\right)^{1/2}\right], \tag{48}$$

$$a = \sqrt{\left|\frac{\delta_e}{A}\right|}, \tag{49}$$

$$b = \sqrt{\left|\frac{\delta_e}{B}\right|}, \tag{50}$$

and

$$\tan 2\alpha = \frac{g_2 \sin 2\sigma}{g_1 - g_2\cos 2\sigma}, \tag{51}$$

where

$$\kappa_\Sigma^{(1)} = \kappa_f^{(h)} + \kappa_h^{(h)},$$

$$\kappa_\Sigma^{(2)} = \kappa_f^{(2)} + \kappa_h^{(2)},$$

$$g_1 = \kappa_f^{(h)} - \kappa_h^{(h)},$$

and

$$g_2 = \kappa_f^{(2)} - \kappa_h^{(2)} \tag{52}$$

The symbol δ_e, which can be obtained from experimental data, represents the elastic deformation of the bearing surfaces. The magnitudes of the major and minor axes of the contact ellipse a and b are expressed in terms of the elastic deformation δ_e. In this study, the value of δ_e is set at 0.00635 mm, which equals the thickness of the coating used for contact pattern rolling testing [8].

10. Example and results

A 12-stop indexing roller gear cam, which has a 30° index period with the modified sine (MS) motion, was selected as an illustrative example to investigate the curvature characteristics and contact ellipse. When the input angle ϕ of the cam rotates from 0° to 360° at a constant angular velocity of 2π rad/s, the turret sequentially processes the following three operations. The first is a dwell period when the input angle ϕ varies from 0° to 30°. The second is 30° indexing period when the input angle ϕ rotates from 30° to 150°, and the last is also a dwell period while the input angle ϕ varies from 150° to 360°, as shown in Fig. 6.

Since the cam mechanism has a single rib, the surfaces I and II are labeled to identify two sides of cam surfaces. Each turret roller behaves in exactly the same manner as every other roller. Although, two adjacent rollers engage different surfaces of the cam track at the same time, only one active cam surface drives follower indexing. These conditions are shown in Fig. 6 as active sections I, II and III.

The basic parameters for the roller gear cam are given as follows: $X_c = 45$ mm, cutter radius $r = 6$ mm, $l_{min} = 21$ mm, $l_{max} = 26$ mm, and the camber roller radius R_c can be 500 or 650 mm (refer Figs. 1–3).

Fig. 7 shows the principal curvatures generated on surfaces I and II during the indexing period. These curvatures intersect with a constant value at the beginning and end points of the indexing period. Obviously, the principle curvatures can be classified into three parts. In the first and third periods, the cutter generates developed rule surfaces and the curvatures are constant in value, or zero. During indexing, the first and second curvatures for surfaces I and II are nearly mirrored at the center point. The first principal curvature was found to vary from 0 to 0.0375946 l/mm, and the second principal curvature from 0 to −0.0495235 l/mm. The difference between the first and second curvatures on the cam surface showed a tendency to increase over the indexing period depending on whether the surface began with a developed rule surface that the first and second curvatures equalled zero.

Fig. 8 shows the contact ellipse on the cam surface under ideal assembly conditions with roller camber radii of 500 and 650 mm, respectively. The major axes of the contact ellipses for the roller camber radius $R_c = 650$ mm were found to be longer than those for $R_c = 500$ mm. A comparison of these camber results in

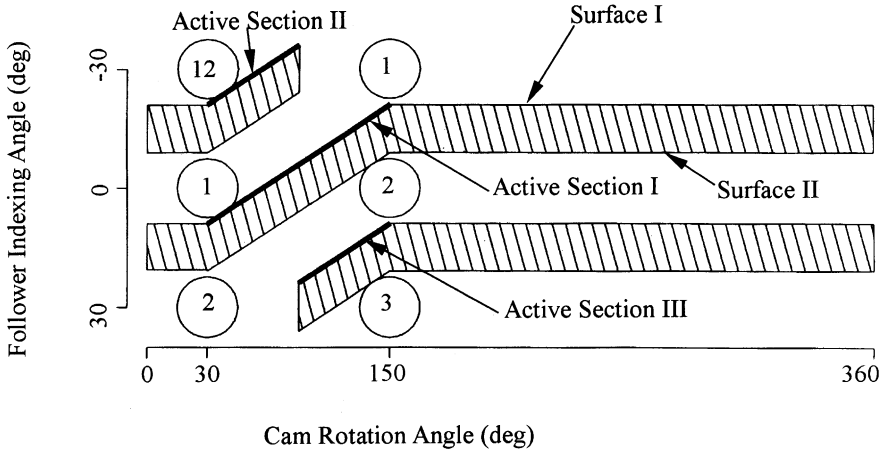

Fig. 6. Schematic diagram of the indexing period.

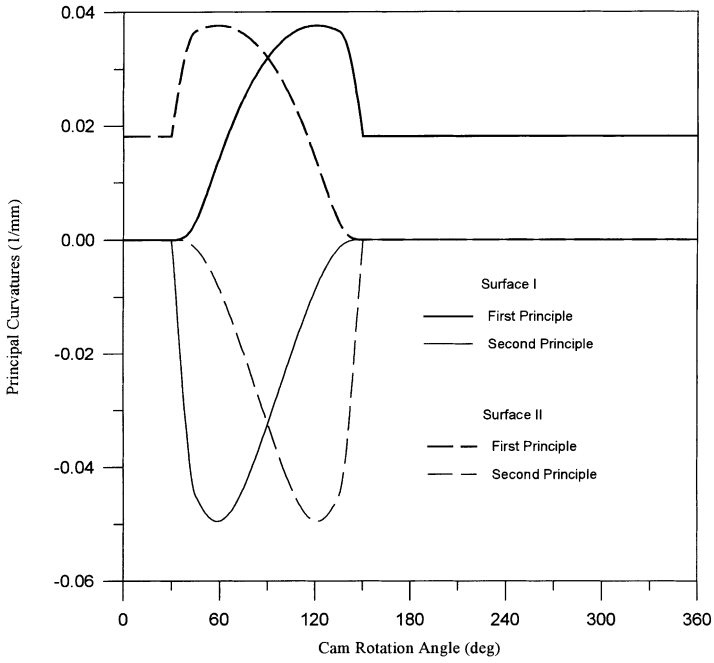

Fig. 7. Comparison of the principal curvatures.

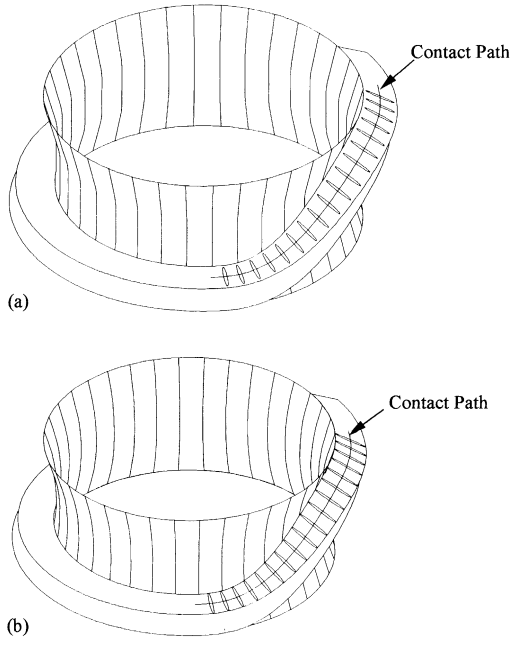

Fig. 8. Contact ellipses on the cam surface: (a) with $R_c = 500$ mm; (b) with $R_c = 500$ mm.

terms of the ratio of semi-major and semi-minor (a/b) of the contact ellipse, is shown as Fig. 9. In the case of the $R_c = 500$ mm, the minimum a/b ratio of the active section I obtained was $a/b = 8.1145$, $a = 1.8259$, $b = 0.2250$, at $\phi = 135°$, the maximum a/b ratio obtained was $a/b = 10.2428$, $a = 2.1662$, $b = 0.2114$, at $\phi = 49°$. Similarly, for $R_c = 650$ mm, the minimum a/b ratio of the active section I obtained was $a/b = 9.2519$, $a = 2.0818$, $b = 0.22502$, at $\phi = 135°$, the maximum a/b ratio obtained was $a/b = 11.6783$, $a = 2.5078$, $b = 0.2147$, at $\phi = 49°$. These results show that the ratio of (a/b) increased over the camber

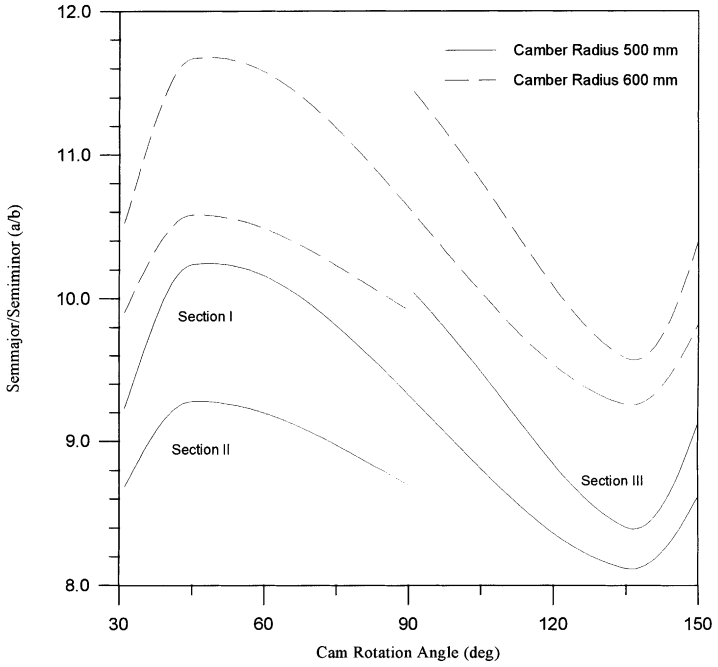

Fig. 9. Comparison on the ratio of semimajor and semiminor axes.

radius, and also indicates that high contact stresses may be induced such that contact ellipses may became longer and narrower.

Fig. 10 shows the variation in the angle σ between the major direction of the contact ellipse and the principal direction of the cam surface. In it we see that the variation in the angle σ is generally symmetrical with the indexing procedure, and the minimum shift angle occurred at the middle, the maximum shift angle is at the two indexing end points.

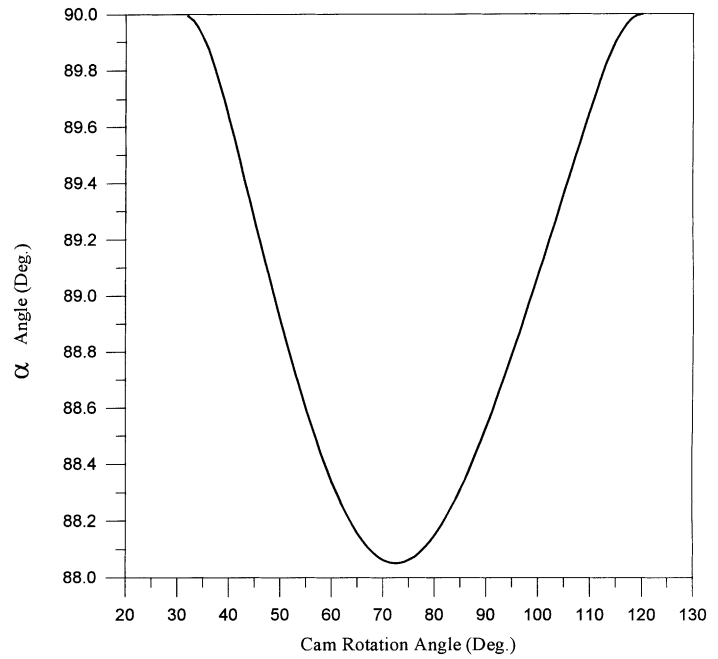

Fig. 10. Shift angle α for the example.

11. Conclusions

In this study, the principal curvatures and directions of the roller gear cam surfaces were investigated. The dimensions and orientations of the contact ellipses for the roller gear cams with a camber roller were calculated based on the Rodrigues' equation and Litvin's studies. The bearing contacts of the roller gear cam were also shown in the illustrative example. It was found that the dimensions and the directions of the contact ellipses affect the contact behaviors and performances of the roller gear cam. The results are most helpful to understand the contact characteristics and lubrication of the roller gear cams, and may be considered as one performance index for the design consideration.

Acknowledgements

The authors are grateful to the National Science Council of the Republic of the China for supporting this research under grant No. NSC 88-2212-E-009-007.

References

[1] M.A. Gonzalez-Palacios, J. Angeles, Generation of contact surfaces of indexing cam mechanism – a unified approach, ASME J. Mech. Des. 116 (2) (1994) 369–374.
[2] J. Chakraborty, S.G. Dhnade, Kinematics and Geometry of Planar and Spatial Cam Mechanisms, Wiley, New York, 1977.
[3] H.S. Yan, H.H. Chen, Geometry design and machining of roller gear cams with cylindrical rollers, Mech. Mech. Theory 29 (6) (1994) 803–812.
[4] H.S. Yan, H.H. Chen, Geometry design of roller gear cams with conical rollers, J. CSME 15 (5) (1994) 479–485.
[5] H.S. Yan, H.H. Chen, Geometry design of roller gear cams with hyperboloidal rollers, Math. Comput. Model. 22 (8) (1995) 107–117.
[6] D.M. Tasy, B.J. Lin, Design and machining of globoidal index cams, ASME J. Manufacturing Sci. Engrg. 119 (1) (1997) 21–29.
[7] T. Oizumi, T. Emura, Globoidal – cam type gearing, in: Proceedings of the 92 International Power Transmission Gearing Conference, vol. 43 (2), ASME Design Engineering Division, New York, 1992, pp. 535–541.
[8] F.L. Litvin, Gear Geometry and Applied Theory, Prentice-Hall, New York, 1994.
[9] F.L. Litvin, C.B. Tsay, Helical gears with circular arc teeth: simulation of conditions of meshing and bearing contact, Trans. ASME J. Mech., Transmissions Automation Des. 107 (1985) 556–564.
[10] F.L. Litvin, N.X. Chen, J.S. Chen, Computerized determination of curvature relations and contact ellipse for conjugate surfaces, Comput. Methods Appl. Mech. Engrg. 125 (1993) 151–170.
[11] W.H. Wang, C.H. Tseng, C.B. Tsay, Surface contact analysis for a spatial cam mechanism, ASME J. Mech. Des. 119 (1) (1997) 169–177.